

Original Article

Fluid Inclusion, Rare-Earth Element and Stable Isotope Study of Carbonate Minerals from the Pongkor Epithermal Gold–Silver Deposit, West Java, Indonesia

I Wayan WARMADA¹, Bernd LEHMANN², Marolop SIMANDJUNTA³ and Herian Sudarman HEMES³

¹Department of Geological Engineering, Gadjah Mada University, Yogyakarta, Indonesia, ²Institute of Mineralogy and Mineral Resources, Technical University of Clausthal, Clausthal-Zellerfeld, Germany and ³PT Aneka Tambang (Persero) Tbk., Unit Penambangan Emas Pongkor, Bogor, Indonesia

Abstract

The Pongkor gold–silver deposit is the largest low-sulfidation epithermal precious metal deposit in Indonesia, and is of Pliocene age. The deposit consists of nine major subparallel quartz–adularia–carbonate veins with very low sulfide content. Vein infill records five paragenetic sequences, dominated by calcite in the early stage and quartz in the later stage of the hydrothermal evolution. Fluid inclusions in hydrothermal calcite and quartz of all stages indicate a temperature ranging from 180 to 220°C and a meteoric water origin (very low salinity close to 0 wt% NaCl equivalent). Carbon isotope data on calcite display a narrow range from –6.5 to –3.0‰ $\delta^{13}\text{C}$. The oxygen isotope values have a wider range of +4.6 to +10.1‰ $\delta^{18}\text{O}$. The broadly positive correlation of the $\delta^{13}\text{C}$ versus $\delta^{18}\text{O}$ plot suggests that the carbon species, which equilibrated during the formation of calcite, is dominated by H_2CO_3 not far from equilibrium with HCO_3^- . The abundance of rare earth and yttrium (REY) in carbonate samples is very low (ΣREY mostly <2 ppm). However, there is always a positive Eu anomaly, which indicates a deeper fluid reservoir at >250°C.

Keywords: carbon, fluid inclusions, hydrothermal, oxygen, rare earth elements, stable isotopes, trace elements.

1. Introduction

Carbonates are the dominant gangue minerals (up to 60%) in the Pongkor gold–silver deposit. They consist of calcite and a small amount of rhodochrosite, kutnahorite, dolomite, ankerite and siderite. The formation of calcite in hydrothermal systems is controlled by $f\text{CO}_2$, pH, temperature, and aqueous calcium ion activity (Fournier, 1985; Simmons & Christenson, 1994). In most present-day geothermal systems $f\text{CO}_2$ appears to be a limiting factor, and the presence or absence of calcite in a hydrothermal mineral assemblage directly reflects the

abundance of carbon dioxide of the coexisting fluid (Giggenbach, 1981, 1988).

This paper presents fluid inclusion, rare-earth element (REE) and carbon and oxygen isotope data of carbonate samples from the Pongkor gold–silver deposit. The aim of the present study was to constrain the physico-chemical conditions of mineralization and the origin of the hydrothermal fluids.

2. Geology and mineralization

The Pongkor area is part of the Neogene Sunda-Banda continental arc that developed along the southern

Received: 31 August 2006. Accepted for publication 6 January 2007.

Corresponding author: I Wayan WARMADA, Department of Geological Engineering, Gadjah Mada University, Jl. Grafika No. 2-Bulaksumur, Yogyakarta 55281, Indonesia. Email: warmada@mail.ugm.ac.id

margin of the Eurasian plate with northward subduction of the Indian–Australian plate. Western Java hosts a number of Cenozoic epithermal precious metal deposits associated with active calc-alkaline volcanism (Fig. 1a, b). They consist of two types of deposits (Marcoux & Milési, 1994): that is, Au–(Sn) deposit of Cirotan type and Au–(Mn) deposit of Pongkor type (Fig. 1b). The 2-Ma Pongkor gold–silver deposit (Milési *et al.*, 1999) is located at the northeastern flank of the Bayah dome, 80 km southwest of Jakarta. The geological unit exposed over an area of approximately 40 × 80 km consists of Late Paleozoic shale and sandstone basement rocks overlain by the central volcanic belt of Oligocene to Early Miocene age, which is composed of largely coarse-grained volcanoclastic rocks, with intercalated limestone and sandstone. Intermediate intrusive rocks are emplaced into Paleogene and Early Miocene formations (Basuki *et al.*, 1994).

The local geology consists of three major volcanic units of Miocene–Pliocene age (Milési *et al.*, 1999). The

lower unit is characterized by submarine calc-alkaline andesitic volcanic rocks grading laterally into epiclastic deposits. The middle unit is marked by more explosive subaerial dacitic volcanic rocks composed of lapilli tuffs overlain by lapilli-and-block tuffs and fine-grained pyroclastic tuffs and epiclastic rocks. The upper unit is formed mainly by andesite lava flows with columnar structure.

The Pongkor deposit consists of at least nine major subparallel quartz–adularia–carbonate veins rich in manganese oxides and limonite in the oxidation zone, and very poor in sulfides. The veins are 740–2700 m long, several meters thick, >200 m deep and cut the three major volcanic units in a fan-like spatial distribution (Fig. 1c).

The main ore components are pyrite, chalcopyrite, sphalerite, galena, electrum, acanthite–aguilarite and polybasite–pearceite, with trace amount of proustite, tetrahedrite and stromeyerite/mckinstryite (Warmada *et al.*, 2003). A trace amount of hessite was reported by

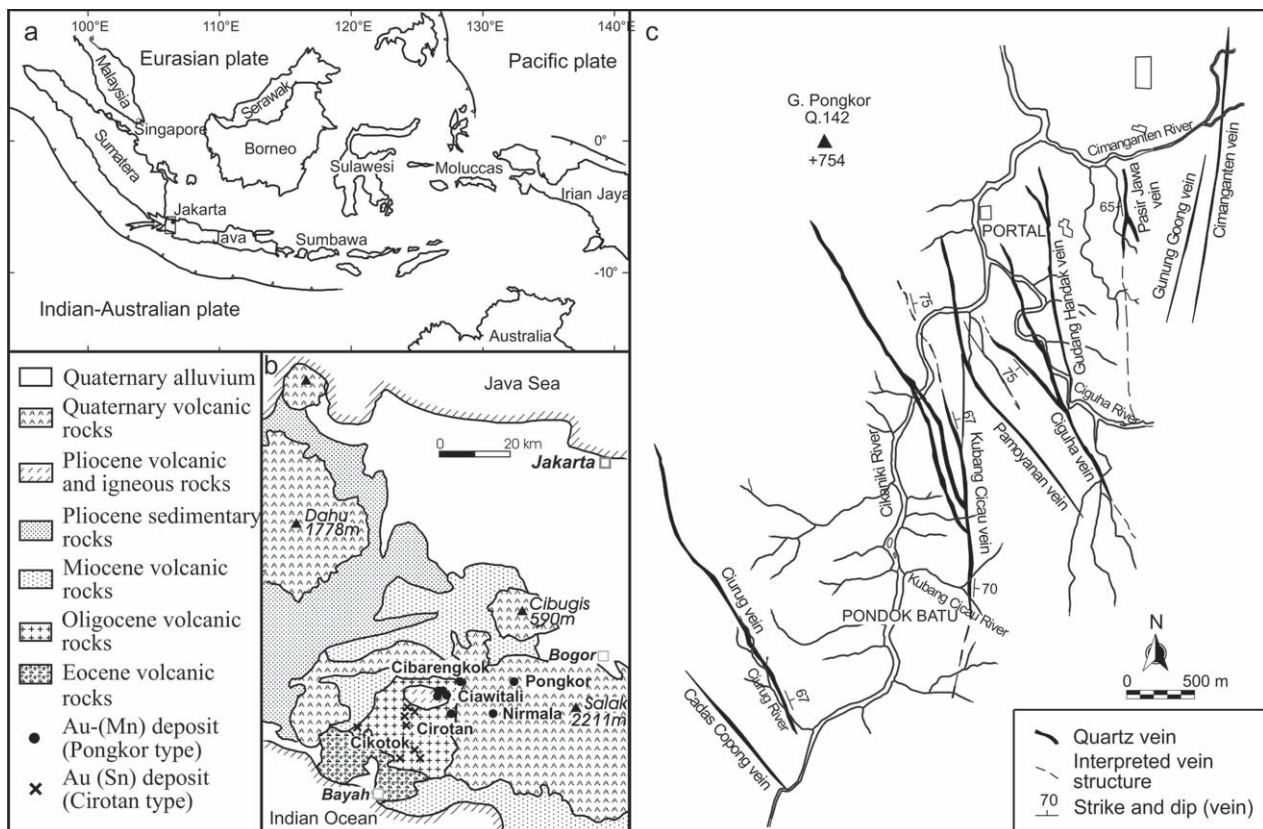


Fig. 1 (a) Tectonic map of the Indonesian region, (b) regional geology of west Java and the location of Pongkor and other major gold deposits (modified from Marcoux & Milési, 1994; Sujatmiko & Santoso, 1992) and (c) pattern of the vein system in the Pongkor gold–silver deposit (PT Aneka Tambang).

Milési *et al.* (1999). Electrum in amoeboid patches and a trace amount of uyttenbogaardtite are the most important gold-bearing mineral and commonly occurs as inclusions in pyrite and more rarely in silver sulfosalts (Greffié *et al.*, 2002; Warmada *et al.*, 2003). Base-metal rich zone has been recognized at the 515-m level of the Ciurug–Cikoret vein (Syafrizal *et al.*, 2005, 2007). The gold content of electrum is around 59 wt% (32–84 wt% Au).

3. Methods

3.1. Samples

The samples were collected from the Ciguha, Ciurug, Gudang Handak, and Kubang Cicau veins (Fig. 1c). The samples from the Ciguha and Gudang Handak veins were obtained from drill cores. The samples of the Ciurug vein were taken from the 515-m level stope and drill cores, whereas the samples from the Kubang Cicau vein were collected from the 550-, 600-, 650- and 690-m level stopes. Forty-five samples were studied in double-polished thin sections, polished thin sections, thin sections and powder, which were selected from different depth levels and from different vein systems.

Double-polished thin sections for fluid-inclusion analysis were made by hand in order to minimize overheating of low-temperature fluid inclusions during sample preparation. All heating and freezing determinations were carried out on a Fluid modified USGS gas-flow heating/freezing stage at the Laboratory of Economic Geology, Technical University of Clausthal, Germany. Its thermocouple was calibrated at temperatures of -56.6 , 0.0 and 374.1°C using Syn Flic synthetic fluid-inclusion standards (Fluid, Denver, USA). During analyses, the thermocouple tip was in contact with the carbonate chips. Freezing rates varied between 1 and $2^{\circ}\text{C}/\text{min}$; heating rates were 1 – $2^{\circ}\text{C}/\text{min}$.

Thirty-four carbonate samples for trace-element and eighteen samples for stable-isotope analysis were crushed to obtain small pieces of carbonate chips. Calcite, rhodochrosite and manganese-rich calcite were hand-picked under a binocular microscope and ground with an agate mortar. Carbonate powder for trace-element analysis was digested with HF and HClO₄ using a CEM Microwave Digestion System at the Laboratory of Economic Geology, Technical University of Clausthal, Germany. The trace-element composition was analyzed by ICP-MS at GeoForschungsZentrum,

Germany. The detection limits in the solution varied from 0.001 to 0.05 ppm.

Carbon and oxygen isotope analyses of calcite were obtained by the phosphoric acid method at room temperature. All C–O isotope analyses were done by the laboratory of Professor Dr J. Hoefs in the Institute of Isotope Geology, Göttingen, Germany. The isotopic composition of CO₂-gas was measured by mass spectrometer with a precision of $\pm 0.2\%$ (Hoefs, 1997). Carbon isotope ratios are reported relative to Pee Dee belemnite (PDB) standard and oxygen isotope ratios are reported relative to standard mean ocean water (SMOW). Isotopic data are reported in the δ notation, $\delta = [(R_{\text{sample}}/R_{\text{standard}}) - 1] \times 1000$, where R is $\delta^{13}\text{C}/^{12}\text{C}$ or $\delta^{18}\text{O}/^{16}\text{O}$, respectively.

4. Results

4.1. Carbonate mineralogy

The principal occurrences of carbonate in the Pongkor are: (i) replacement of rock-forming minerals (especially plagioclase) and volcanic glass; and (ii) vein infill as a main component of the carbonate–quartz stage and the manganese carbonate–quartz stage.

The vein-carbonate material is dominantly composed of fine to coarse crystalline calcite with locally banded rhodochrosite. Three calcite generations are found in the veins. Fine to medium-sized white calcite is formed in the early stage of mineralization, mostly along the footwall and hanging wall of the veins. The second stage of white, brown or honey-colored calcite is more massive and coarsely crystalline. The latest calcite stage, which is mostly coated by iron oxides, filled the fractures of existing veins.

Rhodochrosite [MnCO₃] is mostly altered to manganese oxides and was observed only locally as pink-banded lenses (up to 1 cm thick) in the deeper levels of the Ciguha and Kubang Cicau veins. It is associated with calcite, quartz and banded adularia. Manganian or manganese-rich calcite, with up to 15 wt% Mn is common in Pongkor. The abundant manganese oxide pockets probably result from weathering of these minerals. Dolomite [CaMg(CO₃)₂] and kutnahorite [CaMn(CO₃)₂] are rare and were found only by microprobe analysis. Dolomite occurs as small patchy crystals, probably as a result of local dolomitization processes. Siderite, kutnahorite and ankerite [Ca(Fe,Mg,Mn)(CO₃)₂] are also reported by Milési *et al.* (1999). Prismatic calcite with radial structure is locally found as a void filling in the quartz veins.

Platy (bladed) calcite was found in two varieties: (i) as a network of intersecting bladed infill of voids in quartz veins up to 1.5 cm in size, and (ii) as relicts that vary from submicrometer up to 1 cm in size. The pseudomorph of platy calcite is characterized by coexistence with bladed quartz and clay minerals. The bladed texture appearance of quartz is interpreted as a pseudomorph texture inherited from a platy calcite precursor (Dong *et al.*, 1995). Ghost-blade texture is also found within quartz. Replacement textures of calcite by quartz are very common in the Pongkor vein systems.

4.2. Microthermometry

Fluid inclusions microthermometry was conducted on 34 selected carbonate-quartz samples of quartz-carbonate-adularia veins. The samples were selected from the carbonate-quartz stage, manganese carbonate-quartz stage and gray sulfide-quartz stage (Table 1). The inclusions have irregular to regular-elongated forms, and are mostly of negative crystal shape. They spread parallel to the calcite cleavage as a cluster of inclusions and are interpreted as primary inclusions. There are also fluid inclusions along microfractures, which are classified as secondary inclusions (according

Table 1 Fluid inclusion data and stable isotope composition of carbonate samples

Sample	Depth	Mineral	Type	T _H (°C)	n	T _M (°C)	Salinity (wt% NaCl Eq.)	δ ¹³ C	δ ¹⁸ O
Ciurug									
CRG06	10	Calcite	P	180.4–234.3	15	–0.7 to 0.0	1.23–0.00		
CRG19	80	Calcite	P	212.0–236.2	10	–1.1 to –0.2	1.91–0.35	–4.0	6.8
CRG21	115	Calcite	P	191.4–243.7	11	–0.6 to 0.4	1.05–0.00		
CRG24	95	Quartz	P	180.4–251.4	11	–0.8 to –0.2	1.40–0.35		
CRG25	50	Calcite	P	180.3–249.4	10	–0.4 to 0.1	0.71–0.00		
CRG26	260	Calcite	P	185.1–216.6	10	–0.2 to 0.0	0.35–0.00		
CRG49	165	Calcite	P	183.4–241.8	12	–0.4 to 0.0	0.71–0.00	–5.8	5.7
CRG50	154	Calcite	P	195.2–231.7	12	–0.6 to 0.0	1.05–0.00		
CRG73	200	Calcite	P	185.6–209.8	11	–0.3 to 0.0	0.53–0.00	–4.9	4.9
CRG83	190	Calcite	P	192.2–209.1	13	–1.2 to 0.0	2.07–0.00	–5.6	8.8
CRG88	190	Calcite†	P	190.0–209.9	11	–0.4 to 0.0	0.71–0.00	–4.8	7.3
CRG108.1	200	Quartz	P	202.8–268.9	11	–1.1 to –0.1	1.91–0.18		
CRG108.2	200	Calcite	P	195.6–224.1	11	–1.0 to –0.2	1.74–0.35	–5.6	5.7
Ciguha									
CGH27	183	Quartz	P	181.6–222.3	10	–0.3 to 0.0	0.53–0.00		
CGH28	85	Calcite†	P	187.2–219.7	10	–0.6 to 0.0	1.05–0.00	–6.3	5.2
CGH29	89	Calcite	P	170.9–215.8	11	–1.8 to –0.2	3.06–0.35	–5.2	10.1
CGH43a	60	Calcite	P	204.0–218.6	11	–0.8 to 0.0	1.40–0.00	–6.5	5.2
Kubang Cicau									
KC15	210	Quartz	P	205.4–229.1	8	–1.4 to 0.0	2.41–0.00		
KC54	100	Calcite†	P	171.2–220.2	9	–0.2 to 0.1	0.35–0.00	–3.4	9.7
KC51	45	Quartz	P	190.0–357.1	12	–3.1 to –0.5	5.11–0.88		
KC58	135	Quartz	P	198.8–293.5	6	–0.5 to –0.2	0.88–0.35		
KC62	135	Quartz	P	205.2–330.2	10	–2.5 to –0.2	4.18–0.35		
KC65	165	Calcite	P	193.5–232.4	11	–2.0 to 0.0	3.39–0.00		
KC66a	125	Calcite	P	184.1–231.0	11	–0.5 to 0.0	0.88–0.00	–6.2	5.0
KC66b	210	Quartz	P	191.5–337.1	13	–1.8 to 0.0	3.06–0.00		
KC67	45	Calcite†	P	219.6–226.6	3	–0.8 to –0.1	1.80–0.18	–3.0	8.4
PK198‡	?	Calcite	P	192.0–207.0	10	–0.5 to –0.4	0.88–0.70		
Gudang Handak									
GH91.1	134	Calcite	P	200.6–224.2	11	–1.1 to –0.3	1.91–0.53	–4.8	5.0
GH91.2	134	Quartz	P	207.8–241.2	12	–1.8 to 0.0	3.06–0.00	–5.1	4.7
GH93.1	138	Calcite	P	210.4–248.2	8	–0.8 to –0.1	1.40–0.18		
GH93.2	138	Quartz	P	224.6–269.4	5	–0.3 to –0.2	0.53–0.35	–6.0§	5.3
GH97	35	Calcite	P	189.0–217.8	12	–0.5 to 0.0	0.88–0.00	–5.7	4.6
GH100	34	Calcite	P	202.7–225.5	14	–0.9 to 0.0	1.57–0.00	–5.6	5.2
GH104	33	Calcite†	P	197.5–218.4	11	–0.6 to 0.0	1.05–0.00	–5.8	4.8

T_H, homogenization temperature; T_M, melting temperature. † Manganoan calcite; ‡ Milési *et al.* (1999), § measured in co-genetic calcite.

to the criteria of Roedder, 1984). Some inclusions are also found as single occurrences. Secondary inclusions occur in the variety of platy calcite and have irregular form with flat shape, parallel to the calcite blade/cleavage.

Based on filling ratio, the fluid inclusions can be divided into three types: The SL type represents fluid inclusions composed of a single fluid phase (liquid) without a vapor bubble. The L type is composed of two phase liquid-rich inclusions, and is the dominant fluid inclusion type in both quartz and calcite. The V type inclusions are two phase vapor-rich inclusions with $V/(V + L)$ up to 50%, which are found as primary inclusions in quartz.

The homogenization temperatures (T_H) of the carbonate-hosted fluid inclusions range from 171 to 249°C (maximum frequency, 200°C; arithmetic mean, $205 \pm 15^\circ\text{C}$; $n = 250$) and the melting temperatures (T_M) range from -2.0 to $+0.4^\circ\text{C}$ (maximum frequency, -0.1°C ; arithmetic mean, $-0.3 \pm 0.3^\circ\text{C}$; $n = 234$), which correspond to the salinity from 0 to 3.4 wt% NaCl equivalent. The positive values of some T_M are probably due to ice metastability or CO_2 hydrate formation (Roedder, 1963; Hedenquist & Henley, 1985). The T_H of the quartz-hosted fluid inclusions range from 180 to 357°C (maximum frequency, 220°C; arithmetic mean, $220 \pm 21^\circ\text{C}$; $n = 92$) and the T_M ranges from -3.1 to 0°C (maximum frequency, -0.5°C ; arithmetic mean, $-0.6 \pm 0.6^\circ\text{C}$; $n = 83$), which corresponds to the salinity from 0 to 5.1 wt% NaCl equivalent. Relationships

between the T_H and the T_M for quartz and carbonates from the Ciguha, Ciurug, Gudang Handak and Kubang Cicau veins are presented in Figure 2. No systematic relationship between T_H and depth was observed in the present study, while Syafrizal *et al.* (2005) reported spatial temperature gradient in the Ciurug vein.

4.3. Trace elements

The trace element data for 34 carbonate samples are listed in Table 2. The samples consist of calcite from the Ciurug, Gudang Handak and Kubang Cicau vein systems, and of Mn-rich calcite and rhodochrosite from the Ciguha vein system. Chondrite-normalized rare earth and yttrium patterns (REY; Y inserted between Dy and Ho according to its ionic radius) are generated by using the chondritic values of McDonough and Sun (1995).

The total REY abundances in the carbonate samples are very low (0.41–8.69 ppm), mostly <2 ppm. Carbonate samples with >2 ppm REY also have elevated Zr and Th abundances of >1 ppm Zr and >0.2 ppm Th, suggestive of contamination by accessory minerals or wall-rock particles. There is a slight fractionation of the light REE (LREE) relative to the heavy REE (HREE): $(\text{La}/\text{Yb})_{\text{CN}}$ ranges from 4 to 46. All samples display a slight negative Ce anomaly and a positive Eu anomaly. C1-normalized Eu/Eu^* ratios range up to 63. The Ciguha vein system displays the strongest positive Eu anomalies. These samples consist of Mn-rich calcite to rhodochrosite. The other vein systems display smaller positive Eu anomalies.

The samples display Y/Ho ratios within the range from 29 to 69, which are mostly significantly higher than those of chondrite of 26–28. The samples with the lowest Y/Ho ratio are also those that have the highest REY, Zr and Th abundances, that is, are controlled by accessory phases or wall-rock contamination. All samples have a slightly positive Y anomaly. The altered andesitic wall rocks have a slight negative Eu anomaly (Fig. 2). The scatter in some samples with very low HREE contents is due to the reduced analytical precision near the detection level (Table 2).

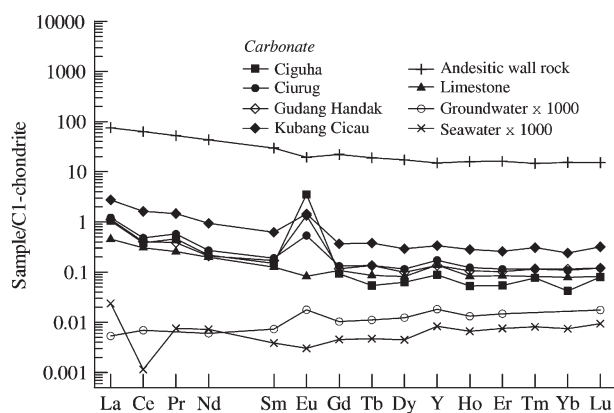


Fig. 2 Average rare-earth element (REE) patterns of carbonate from the Pongkor gold-silver deposit compared with reference rocks and fluids. Source of reference data: limestone from Dulski (2001), seawater from geochemical Earth reference model (GERM) online database, and groundwater from Möller *et al.* (1997).

4.4. Carbon and oxygen isotopes

The carbonate samples consist of manganoan calcite to pure calcite and were selected randomly from four vein systems. The $\delta^{18}\text{O}$ and $\delta^{13}\text{C}$ data are given in Table 1.

No distinct difference in oxygen and carbon isotope composition is observed between individual vein systems and individual stages. The carbon isotopic composition of the carbonate samples spans a narrow range of $\delta^{13}\text{C}_{\text{PDB}}$ values between -6.5 and -3.0‰ (mean $-5.3 \pm 1.0\text{‰}$). The equilibrium $\delta^{13}\text{C}$ composition of carbon dioxide for most of these data falls between -5.6 and -1.7‰ , calculated on the basis of fractionation factors of Chacko *et al.* (1991) (Fig. 3a). The oxygen isotope values have a wider range with $\delta^{18}\text{O}_{\text{SMOW}}$ values between $+4.6$ and $+10.1\text{‰}$ (mean $+6.3 \pm 1.8\text{‰}$). Taking the calcite Th data of calcite as representative thermal conditions of isotopic equilibration, the equilibrium $\delta^{18}\text{O}$ value of water ranging from -3.4 to $+1.5\text{‰}$, were calculated on the basis of fractionation factors of Zheng (1993) (Fig. 3b).

5. Discussion

5.1. Evidence for boiling

The Pongkor epithermal system formed from very low-salinity ore fluid at temperatures of 180 – 220°C . The presence of vapour-rich fluid inclusions in quartz could be evidence of boiling. The presence of rhombic adularia in the bonanza ore and rhodochrosite could be evidence for boiling (Plumlee, 1994). Tabular adularia occurs as a band up to 1 mm thick, interbedded or interfingering with banded quartz or microcomb quartz. Such adularia has been reported from epithermal systems in central Queensland, Australia (Dong & Morrison, 1995), where adularia gave Th between 264 and 278°C , and was interpreted as resulting from boiling judged by disordered Al/Si distribution of adularia (Dong & Morrison, 1995).

The presence of platy calcite also indicates boiling (Simmons & Christenson, 1994). It is interesting to note that the vapor-rich end members of the boiling system were not observed in primary fluid inclusions of calcite. This may be a consequence of the shallow ore environment (open system), in which the vapor phase moves much more rapidly and is correspondingly much less likely to become trapped.

The majority of the carbonate-hosted inclusions melt at an average temperature of -0.3°C , indicating an apparent salinity of 1 wt% NaCl equivalent. There are also a small number of inclusions with moderate apparent salinities (2 – 5 wt% NaCl equiv.). The co-existence of moderate-salinity inclusions with low-salinity inclusions can be explained as the result of extensive boiling and vaporization of low-salinity fluid

(Simmons & Browne, 1997; Scott & Watanabe, 1998), but it can also result from mixing of two fluids of different salinity.

Although the $V/(L + V)$ ratio of the fluid inclusions is generally low, trends in Figure 4 suggest that boiling and mixing of fluids occurred during calcite and quartz precipitation. The trends are close to a schematic model proposed by Hedenquist and Henley (1985) and Ruggieri *et al.* (2001). The schematic positive gradient of T_M versus Th in Figure 4 (trend C) is due to the loss of steam. A negative gradient (trend B) would result from mixing between the main fluid and a very low-salinity fluid. Loss of steam is possible in a shallow open system, where the vapor-rich inclusions cannot be trapped in crystals. The trend A is fluid cooling at constant salinity.

Given the mineralogical evidence of boiling and the fact that T_M versus Th patterns suggest boiling, no pressure corrections are required for the Th. Otherwise, the pressure correction would be on the order of 10 – 20°C , taking into account the young age of the deposit and an erosion rate of 0.1 mm/year, typical of Cenozoic island arcs (Hedenquist *et al.*, 2000). Based on the liquid–vapor curve of water (Haas, 1971), the hydrostatic depth of a boiling system at 180 – 220°C is 100 – 250 m, assuming a low-salinity fluid and no dissolved CO_2 .

The decreasing of P_{CO_2} on boiling, as carbon dioxide is lost to the steam phase, increases the pH of the solution and leads to supersaturation and precipitation of calcite.

5.2. REE distribution patterns

The REE characteristics of hydrothermal carbonates are controlled by the composition of the fluid and physicochemical conditions during precipitation (Bau & Möller, 1992). Variation in growth rate or solution flow rates may affect the total REE contents of carbonates (Möller *et al.*, 1997). The REE composition of the fluid depends on degree of fluid–rock interaction and abundance of complexing species, that is, HCO_3^- , CO_3^{2-} , Cl^- , and OH^- . The mobility of REE in hydrothermal fluids may be largely influenced by sorption processes and chemical complexation during fluid migration (Bau & Möller, 1992).

The extremely low content of REY in the carbonate samples suggests that the fluid had low REY contents, although the carbon and oxygen isotope data suggest that there was water–rock interaction between wall rocks and fluid (meteoric water). The low REY contents

Table 2 Trace element composition of selected carbonate samples

	CGH28	CGH42	CGH43	CRG21	CRG25	CRG26	CRG50.2	CRG72	CRG73	CRG74	CRG75
Depth (m)	85	129	62	115	50	260	154	190	200	200	200
Rb (ppm)	1.73	3.14	0.606	4.064	8.33	5.08	0.717	1.33	0.133	0.309	0.222
Sr	86.4	354	274	94.5	269	277	402	298	245	230	240
Y	0.195	0.183	0.121	0.303	0.213	0.298	0.273	0.158	0.294	0.934	0.254
Zr	0.994	0.497	0.229	0.36	1.10	1.10	0.912	0.977	0.615	0.918	0.778
Cs	1.97	0.211	2.07	0.515	0.752	0.483	0.051	0.173	0.05	0.382	0.064
Ba	6.15	3.25	3.13	7.10	8.26	7.07	7.49	4.53	3.75	3.96	3.22
La	0.224	0.309	0.303	0.147	0.627	0.582	0.252	0.18	0.196	0.262	0.357
Ce	0.229	0.419	0.268	0.176	1.042	1.043	0.232	0.119	0.113	0.216	0.277
Pr	0.028	0.073	0.047	0.042	0.150	0.140	0.052	0.029	0.040	0.039	0.044
Nd	0.091	0.189	0.110	0.092	0.416	0.424	0.111	0.049	0.078	0.087	0.122
Sm	0.021	0.037	0.023	0.029	0.080	0.082	0.026	0.016	0.027	0.025	0.027
Eu	0.356	0.079	0.254	0.030	0.034	0.044	0.033	0.029	0.011	0.024	0.072
Gd	0.025	0.031	0.017	0.033	0.056	0.061	0.029	0.015	0.027	0.045	0.025
Tb	0.003	0.004	0.002	0.006	0.008	0.009	0.006	0.002	0.005	0.007	0.003
Dy	0.017	0.029	0.014	0.045	0.042	0.053	0.037	0.017	0.031	0.058	0.024
Ho	0.003	0.005	0.002	0.010	0.007	0.010	0.007	0.004	0.007	0.015	0.005
Er	0.01	0.016	0.007	0.025	0.021	0.031	0.020	0.013	0.023	0.049	0.013
Tm	<0.002	<0.002	<0.002	0.004	0.003	0.005	0.003	0.002	0.003	0.005	0.002
Yb	0.005	0.015	0.005	0.023	0.019	0.031	0.017	0.011	0.023	0.030	0.011
Lu	<0.002	<0.002	<0.002	0.003	0.003	0.004	0.003	0.002	0.003	0.004	0.002
Hf	<0.05	<0.05	<0.05	<0.05	<0.05	<0.05	<0.05	0.022	0.013	0.018	0.014
Pb	57.0	2.77	1.86	76.7	1.38	1.32	0.907	4.13	3.94	9.68	2.96
Th	0.036	0.066	<0.03	<0.03	0.241	0.218	<0.03	0.007	0.009	0.009	0.007
U	0.007	0.021	<0.02	0.006	0.034	0.046	0.006	0.01	0.009	0.02	0.008
ΣREY	1.21	1.39	1.17	0.968	2.72	2.82	1.10	0.646	0.881	1.80	1.24
(La/Yb) _N	32.2	15.3	46.1	4.79	24.3	13.7	11.3	12.5	6.20	6.53	24.4
(La/Sm) _N	7.38	5.75	8.95	3.46	5.33	4.84	6.54	7.71	5.00	7.01	9.08
(Tb/Yb) _N	2.33	1.32	2.19	1.25	1.98	1.31	1.59	0.881	0.859	1.06	1.13
Eu/Eu*	47.9	6.98	37.2	2.94	1.48	1.80	3.57	5.50	1.25	2.12	8.33
Ce/Ce*	0.557	0.619	0.460	0.506	0.756	0.813	0.441	0.341	0.277	0.433	0.426
Y/Ho	58	35	49	32	31	30	37	40	40	61	47

REY, rare earth and yttrium.

in calcite and, by inference, in the hydrothermal fluid, suggest a relatively short residence time of the meteoric water aquifer, that is, fast recharge.

The partition coefficients of REE in calcite decrease systematically with increasing REE atomic number (Zhong & Mucci, 1995). The slightly enriched LREE and depleted HREE patterns of the carbonate from the Pongkor gold–silver deposit are probably controlled by the affinity of those elements to calcite cation sites. Based on experimental studies of the distribution coefficient of the calcite–water system, the REE abundance in the hydrothermal fluid could have been 0.001–1-fold the REE content in calcite. The wide range of the REE partition coefficients is due to conflicting experimental data (Parekh *et al.*, 1977; Terakado & Masuda, 1988; Zhong & Mucci, 1995).

The negative Ce anomalies are typical of marine carbonates and seawater, and reflect oxidizing conditions. The low salinity of the Pongkor hydrothermal system

excludes involvement of seawater, and points to oxidized meteoric water.

The carbonate samples display a range of Eu anomalies, that is, from no Eu anomaly to strongly positive Eu anomaly (Fig. 2). The Eu anomalies are likely to directly reflect the $\text{Eu}^{2+}/\text{Eu}^{3+}$ ratio in the fluid (Zhong & Mucci, 1995). The $\text{Eu}^{2+}/\text{Eu}^{3+}$ ratio in a rock-buffered fluid is strongly dependent on temperature, and $\text{Eu}^{2+}/\text{Eu}^{3+}$ equilibrium is established at around 250°C (Sverjensky, 1984; Bau & Möller, 1992). Positive Eu anomalies in a fluid therefore need a temperature of more than approximately 250°C, that is, the positive Eu anomaly in most calcite samples reflects higher temperature than recorded during calcite deposition and points to deeper fluid–rock interaction at a higher reservoir temperature than seen in the fluid inclusions trapped at near-surface environment.

The positive Eu anomaly in the carbonate samples could also be due to breakdown of plagioclase in the

CRG83	CRG88	CRG108	GH91	GH93	GH100	GH102	GH105	KC52.1	KC52.2	KC54	KC66.1	KC67
200	190	180	134	138	34	33	34	50	50	100	210	45
0.114	0.407	0.251	0.420	18.6	0.157	1.72	5.69	1.07	57.0	0.711	14.6	1.22
227	825	121	204	313	426	461	247	559	222	286	140	217
0.165	0.218	0.458	0.143	0.164	0.102	0.784	0.209	0.415	1.28	0.882	0.393	0.452
0.631	1.47	0.622	0.315	0.860	0.364	0.805	0.489	0.604	4.53	0.53	1.77	0.220
0.026	0.233	0.091	0.274	1.08	0.049	0.164	0.324	0.057	2.32	0.078	0.929	0.104
3.87	6.48	4.31	2.74	34.1	1.90	5.62	19.8	2.73	50.7	5.39	11.2	2.45
0.186	0.123	0.157	0.234	0.191	0.174	0.586	0.280	0.627	1.49	0.275	1.03	0.258
0.157	0.083	0.128	0.188	0.187	0.142	0.758	0.316	0.976	2.92	0.254	1.89	0.199
0.034	0.026	0.033	0.030	0.029	0.021	0.095	0.044	0.123	0.369	0.048	0.233	0.047
0.061	0.026	0.041	0.061	0.064	0.054	0.322	0.126	0.370	1.349	0.140	0.743	0.108
0.015	0.012	0.015	0.013	0.015	0.013	0.084	0.027	0.090	0.310	0.033	0.133	0.027
0.071	0.009	0.022	0.084	0.017	0.016	0.066	0.154	0.100	0.131	0.037	0.151	0.028
0.015	0.011	0.028	0.012	0.014	0.012	0.095	0.026	0.075	0.235	0.052	0.094	0.023
0.002	0.003	0.006	0.001	0.002	0.002	0.015	0.004	0.011	0.039	0.010	0.014	0.004
0.012	0.022	0.044	0.014	0.014	0.013	0.100	0.029	0.055	0.235	0.073	0.079	0.032
0.003	0.004	0.012	0.003	0.004	0.002	0.022	0.005	0.011	0.044	0.017	0.013	0.007
0.011	0.016	0.033	0.010	0.012	0.007	0.068	0.019	0.030	0.131	0.056	0.038	0.024
0.002	0.002	0.005	0.001	0.002	<0.001	0.009	0.003	0.004	0.019	0.009	0.005	0.003
0.010	0.015	0.029	0.011	0.011	0.007	0.065	0.018	0.028	0.121	0.055	0.034	0.023
0.001	0.002	0.004	0.001	0.001	0.001	0.011	0.004	0.004	0.019	0.007	0.005	0.003
0.012	0.030	0.012	0.006	0.017	0.008	0.020	0.011	<0.05	<0.05	<0.05	<0.05	<0.05
14.2	8.70	5.09	7.36	8.91	2.19	80.3	7.69	0.748	19.1	1.38	1.85	0.526
0.005	0.01	0.007	0.011	0.006	0.008	0.03	0.013	0.109	0.502	<0.03	0.339	<0.03
0.006	0.011	0.009	0.007	0.014	0.007	0.012	0.009	0.030	0.184	0.115	0.081	0.025
0.745	0.572	1.02	0.806	0.727	0.566	3.08	1.26	2.92	8.69	1.95	4.85	1.24
14.3	6.18	4.08	16.5	13.0	18.9	6.65	11.4	16.5	9.11	3.68	22.1	8.38
8.64	6.76	7.37	12.2	8.79	9.04	4.75	7.12	4.77	3.28	5.78	5.28	6.47
0.788	0.763	0.920	0.412	0.649	1.27	1.00	1.01	1.71	1.41	0.762	1.83	0.754
14.4	2.38	3.26	20.5	3.62	3.82	2.24	17.7	3.63	1.42	2.76	3.95	3.39
0.419	0.320	0.387	0.438	0.509	0.451	0.665	0.585	0.757	0.879	0.465	0.855	0.385
57	55	39	49	43	44	36	38	38	29	53	29.7	68.9

country rock as seen by hydrothermal alteration of plagioclase in the wall rock and formation of hydrothermal carbonate and adularia. There is a slight negative Eu anomaly in the altered andesitic country rock, which could reflect hydrothermal Eu depletion and complementary Eu enrichment in the fluid.

The Y/Ho ratios of the carbonate samples (29–69) are significantly higher than those of chondrite or igneous and sedimentary rocks (26–28) and are typical of hydrothermal systems (Bau & Dulski, 1995).

5.3. Carbon and oxygen isotopes

The isotope composition of carbonates is controlled by carbon-bearing species in solution as well as by temperature (Ohmoto, 1972). The solubility of calcite in a low-salinity hydrothermal fluid decreases with increasing temperature, and increases with increasing P_{CO_2} (Rimstidt, 1997). Therefore, degassing of CO_2

can be an effective process responsible for calcite precipitation (Rimstidt, 1997). The $\delta^{13}C$ and $\delta^{18}O$ values of a H_2CO_3 - and HCO_3^- -dominated fluid can be estimated by a Rayleigh degassing-precipitation model, which is frequently applied to the interpretation of carbon isotope variations (Valley, 1986; Zheng, 1990).

A plot of $\delta^{13}C_{calcite}$ versus $\delta^{18}O$ data in Figure 5 shows two calcite precipitation models, which were calculated based on a Rayleigh-degassing precipitation model with the initial fluid values of -4% for $\delta^{18}O$ and -6.5% for $\delta^{13}C$ (HCO_3^- -dominated fluid) and -5.5% (H_2CO_3 -dominated fluid), respectively. These initial fluid values are derived by an iterative model that adjusts the fractionation lines to the data set (Zheng, 1993).

The positive correlation between $\delta^{13}C$ and $\delta^{18}O$ of manganoan calcite is likely to be caused by the precipitation of Mn-rich calcite from a H_2CO_3 -dominated fluid accompanied by progressive decrease in

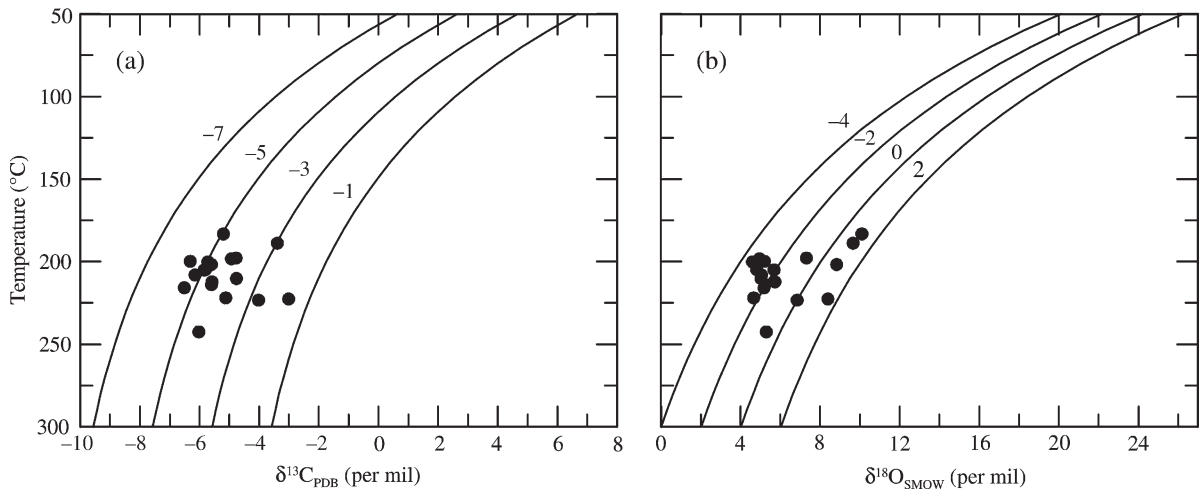


Fig. 3 Stable isotope data of calcite: (a) $\delta^{13}\text{C}$ composition of calcite versus homogenization temperature (T_H). Isoleths show the calculated $\delta^{13}\text{C}$ per mil values of aqueous carbon dioxide in equilibrium with calcite as a function of temperature, calculated on the basis of fractionation factors of Chacko *et al.* (1991), (b) $\delta^{18}\text{O}$ composition of calcite versus homogenization temperature (T_H). Isoleths show the calculated $\delta^{18}\text{O}$ per mil values of water in equilibrium with calcite as a function of temperature, calculated on the basis of fractionation factors of Zheng (1993). PDB, Peedee belemnite; SMOW, standard mean ocean water.

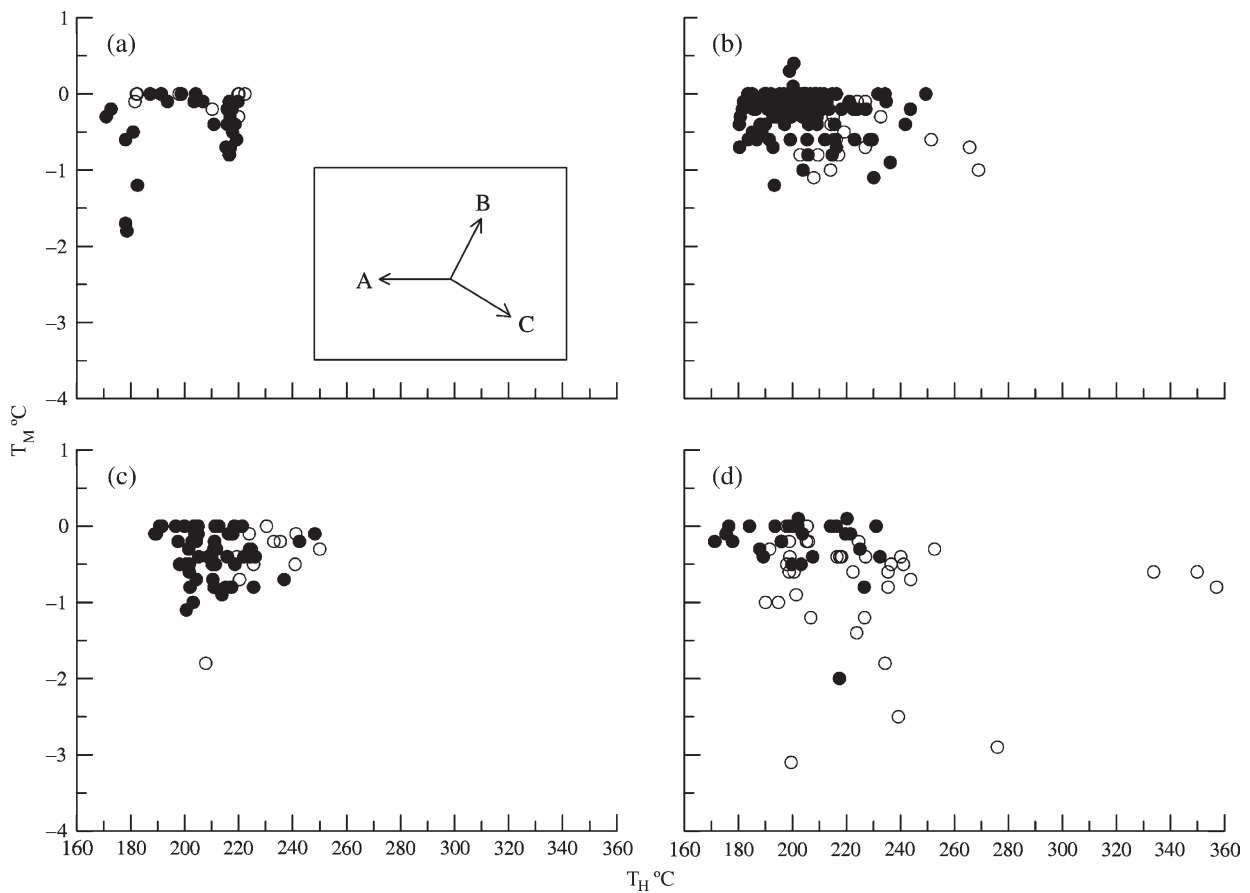


Fig. 4 Scatter plot of homogenization temperature (T_H) versus melting temperature (T_M). (a) Ciguha; (b) Ciurug; (c) Gudang Handak; (d) Kubang Cicau. (•) Carbonate; (o) quartz. Trend A: fluid cooling. Trend B: mixing. Trend C: boiling.

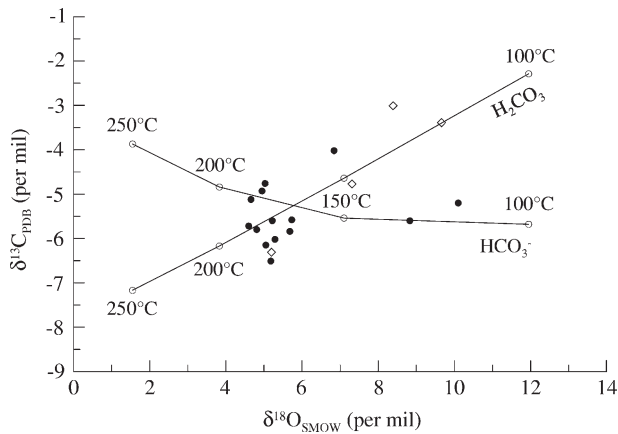


Fig. 5 Carbon and oxygen isotope composition of calcite from the Pongkor gold-silver deposit. Theoretical curves for calcite composition are calculated using a Rayleigh degassing-precipitation model with HCO_3^- and H_2CO_3 , respectively, as the dominant dissolved carbon species in the fluid. The $\delta^{18}\text{O}$ of the fluid is taken as -4‰ , the $\delta^{13}\text{C}$ as -6.5‰ for HCO_3^- -dominated fluid and -5.5‰ for H_2CO_3 -dominated fluid; the mol fraction of carbon in degassed CO_2 is taken as 0.05 and that of oxygen as 0.005. (•) Calcite; (◊) manganocalcite; (○) calculated model. SMOW, standard mean ocean water.

temperature during CO_2 degassing. Most carbonate samples display a scatter distribution with an elongated horizontal trend, typical of HCO_3^- -dominated fluids. Because no trace of gas was detected in the fluid inclusions during microthermometry measurements and by Raman microspectrometry (Milési *et al.*, 1999), only pH and temperature are assumed to control the speciation of H_2CO_3 and HCO_3^- (Lüders & Möller, 1992).

The change from slightly acid (H_2CO_3) to fairly neutral pH (HCO_3^-) is reflected by the Mn/Ca ratio of calcite (Johnson, 1982). The changing ratio, observed at Pongkor, could be explained by mixing of two fluids with different pH, but variable pH could also result from boiling. Progressive change in pH was also reported by Milési *et al.* (1999) deduced from carbonate zoning in the Ciguha vein, from siderite (low pH), to Mn-Mg carbonate and finally calcite (fairly neutral pH).

The $\delta^{18}\text{O}$ value of carbonate samples displays a wider range than for the $\delta^{13}\text{C}$ value. The variation in the $\delta^{18}\text{O}$ values of the carbonates suggests variable degree of wall-rock interaction of the fluids and/or temperatures of equilibration. The present-day oxygen isotope composition of Java rainwater is approximately -5 to -6‰ $\delta^{18}\text{O}$ (IAEA, 2001). Given an oxygen isotope composition of the volcanic host rocks of

approximately $+8\text{‰}$ $\delta^{18}\text{O}$, the degree of oxygen exchange of the hydrothermal fluid system is between 10 and 50%.

6. Conclusions

Fluid inclusions in hydrothermal calcite define a temperature of formation of around 200°C and a meteoric water origin (very low salinity). There is no evidence of boiling observed in calcite from the fluid inclusion petrography. However, the presence of vapor-rich fluid inclusions in quartz, rhombic adularia, and lattice quartz texture replacing bladed calcite are interpreted as evidence for boiling. The absence of vapor-rich inclusions in calcite is probably due to the shallow ore-forming environment, in which the vapor phase moves rapidly (open system).

The REY content of carbonates is very low (<2 ppm). Some samples with higher REY content up to 8.7 ppm are probably caused by particles derived from host rocks (elevated Th and Zr contents, Y/Ho around 30). The very low REY abundance in calcite reflects a low REY content in the hydrothermal fluid, which is related to the low complexing capacity of the low-salinity fluid. The REY patterns display slightly negative Ce anomalies, positive Eu anomalies and positive Y anomalies. The negative Ce anomalies reflect an oxidizing environment. The positive Eu anomalies suggest that the initial fluid attained a minimum temperature of 250°C , which indicates water-rock interaction at higher temperature in a deeper reservoir. The positive Y anomalies reflect the aqueous environment in which Y and Ho become fractionated.

The carbon isotope composition of calcite has a narrow range with $\delta^{13}\text{C}$ values between -6.5 and -3.0‰ (mean $-5.2 \pm 1.0\text{‰}$), whereas the oxygen isotope values have a wider range of $\delta^{18}\text{O}$ with values between $+4.6$ and $+10.1\text{‰}$ (mean $+6.3 \pm 1.8\text{‰}$). The positive linear correlation between $\delta^{13}\text{C}$ and $\delta^{18}\text{O}$ values of manganocalcite suggests that the Mn-rich calcite was deposited from a H_2CO_3 -dominated fluid. Scatter distribution of carbonate samples with an elongated horizontal trend is typical of HCO_3^- -dominated fluids. The stable isotope data indicate variable pH in the system, which likely resulted from boiling or mixing.

Acknowledgments

This contribution is part of a PhD project financed by Deutscher Akademischer Austauschdienst (DAAD). We gratefully acknowledge permission from PT Aneka

Tambang (Persero) Tbk to work in the Pongkor mine and to publish these results, and the help of Eko Janu Herlambang in the field, Klaus Herrmann (TU Clausthal) during electron microprobe analysis. We also thank Volker Lüders for useful discussion. The ICP-MS analysis was done by Peter Dulski (GFZ Potsdam). We also wish to thank the two anonymous reviewers for constructive reviews, which helped clarify the focus of this paper and especially, Akira Imai who helped to significantly improve and clarify the original text.

References

- Basuki, A., Sumanagara, D. A. and Sinambela, D. (1994) The Gunung Pongkor gold-silver deposit, West Java, Indonesia. *J. Geochem. Explor.*, 50, 371–391.
- Bau, M. and Dulski, P. (1995) Comparative study of yttrium and rare-earth element behaviours in fluorite-rich hydrothermal fluids. *Contrib. Mineral. Petrol.*, 119, 213–223.
- Bau, M. and Möller, P. (1992) Rare earth element fractionation in metamorphogenic hydrothermal calcite, magnesite and siderite. *Mineral. Petrol.*, 45, 231–246.
- Chacko, T., Mayeda, T. K., Clayton, R. N. and Goldsmith, J. R. (1991) Oxygen and carbon isotope fractionations between CO₂ and calcite. *Geochim. Cosmochim. Acta*, 55, 2867–2882.
- Dong, G. and Morrison, G. W. (1995) Adularia in epithermal veins, Queensland: Morphology, structural state and origin. *Mineral. Deposita*, 30, 11–19.
- Dong, G., Morrison, G. W. and Jaireth, S. (1995) Quartz textures in epithermal veins, Queensland: Classification, origin, and implication. *Econ. Geol.*, 90, 1841–1856.
- Dulski, P. (2001) Reference materials for geochemical studies: New analytical data by ICP-MS and critical discussion of reference values. *Geostandards Newslett.*, 25, 87–125.
- Fournier, R. O. (1985) Carbonate transport and deposition in the epithermal environment. *Rev. Econ. Geol.*, 2, 63–71.
- Giggenbach, W. F. (1981) Geothermal mineral equilibria. *Geochim. Cosmochim. Acta*, 45, 393–410.
- Giggenbach, W. F. (1988) Geothermal solute equilibria. Derivation of Na-K-Mg-Ca geothermometers. *Geochim. Cosmochim. Acta*, 52, 2749–2765.
- Greffié, C., Bailly, L. and Milési, J. P. (2002) Supergene alteration of primary ore assemblages from low-sulfidation Au-Ag epithermal deposits at Pongkor, Indonesia, and Nazareño, Perú. *Econ. Geol.*, 97, 561–571.
- Haas, J. L. (1971) The effect of salinity on the maximum thermal gradient of hydrothermal system at hydrostatic pressure. *Econ. Geol.*, 66, 940–946.
- Hedenquist, J. W. and Henley, R. W. (1985) The importance of CO₂ on freezing point measurements of fluid inclusions: Evidence from active geothermal systems and implications for epithermal ore deposition. *Econ. Geol.*, 80, 1379–1406.
- Hedenquist, J. W., Arribas, A. Jr. and Gonzalez-Urien, E. (2000) Exploration for epithermal gold deposits. *Rev. Econ. Geol.*, 13, 245–277.
- Hoefs, J. (1997) *Stable isotope geochemistry*, 4th ed. Springer-Verlag, Berlin, 201p.
- IAEA (2001) GNIP maps and animation. International Atomic Energy Agency, Vienna. (Accessed 23 May 2005.) Available from URL: <http://isohis.iaea.org/userupdate/waterloo/South%20Pacific/slide01.gif>
- Johnson, K. S. (1982) Solubility of rhodochrosite (MnCO₃) in water and seawater. *Geochim. Cosmochim. Acta*, 46, 1805–1809.
- Lüders, V. and Möller, P. (1992) Fluid evolution and ore deposition in the Harz Mountains (Germany). *Eur. J. Mineral.*, 4, 1053–1068.
- Marcoux, E. and Milési, J. P. (1994) Epithermal gold deposits in West Java, Indonesia: Geology, age and crustal source. *J. Geochem. Explor.*, 50, 393–408.
- McDonough, W. F. and Sun, S.-S. (1995) The composition of the earth. *Chem. Geol.*, 120, 223–253.
- Milési, J. P., Marcoux, E., Sitorus, T., Simandjuntak, M., Leroy, J. and Bailly, L. (1999) Pongkor (west Java, Indonesia): A Pliocene supergene-enriched epithermal Au-Ag-(Mn) deposit. *Mineral. Deposita*, 34, 131–149.
- Möller, P., Stober, I. and Dulski, P. (1997) Seltenerdelement-, Yttrium-Gehalte und Bleisotope in Thermal- und Mineralwässern des Schwarzwaldes. *Grundwasser*, 3, 118–131.
- Ohmoto, H. (1972) Systematics of sulfur and carbon isotopes in hydrothermal ore deposits. *Econ. Geol.*, 67, 551–578.
- Parekh, P. P., Möller, P. and Dulski, P. (1977) Distribution of trace elements between carbonate and non-carbonate phases of limestone. *Earth Planet. Sci. Lett.*, 34, 39–50.
- Plumlee, G. S. (1994) Fluid chemistry evolution and mineral deposition in the main-stage Creed epithermal system. *Econ. Geol.*, 89, 1860–1882.
- Rimstidt, J. D. (1997) Gangue mineral transport and deposition. In Barnes, H. L. (ed.) *Geochemistry of hydrothermal ore deposits*, 3rd edn. Wiley, New York, 487–515.
- Roedder, E. (1963) Studies of fluid inclusion II: Freezing data and their interpretation. *Econ. Geol.*, 58, 167–211.
- Roedder, E. (1984) Fluid inclusions. *Rev. Mineral.*, 12, 644.
- Ruggieri, G., Cathelineau, M., Boiron, M. C. and Marignac, C. (2001) Boiling and fluid mixing in the chlorite zone of the Larderello geothermal system. *Chem. Geol.*, 154, 237–256.
- Scott, A. M. and Watanabe, Y. (1998) “Extreme boiling” model for variable salinity of the Hokko low-sulfidation epithermal Au prospect, southwestern Hokkaido, Japan. *Mineral. Deposita*, 33, 568–578.
- Simmons, S. F. and Browne, P. R. L. (1997) Saline fluid inclusions in sphalerite from the Broadlands-Ohaaki geothermal system: A coincidental trapping of fluids boiled towards dryness. *Econ. Geol.*, 92, 485–489.
- Simmons, S. F. and Christenson, B. W. (1994) Origin of calcite in a boiling geothermal system. *Am. J. Sci.*, 294, 361–400.
- Sujatmiko, and Santoso, S. (1992) The geologic map of the Leuwidamar Quadrangle, Jawa. Pusat Penelitian dan Pengembangan Geologi.
- Sverjensky, D. A. (1984) Europium redox equilibria in aqueous solution. *Earth Planet. Sci. Lett.*, 67, 70–78.
- Syafrizal, Imai, A., Motomura, Y. and Watanabe, K. (2005) Characteristics of gold mineralization at the Ciurug vein, Pongkor gold-silver deposit, West Java, Indonesia. *Resour. Geol.*, 55, 225–238.
- Syafrizal, Imai, A. and Watanabe, K. (2007) Origin of ore-forming fluids responsible for gold mineralization of the Pongkor

- Au-Ag deposit, West Java, Indonesia: Evidence from mineralogic, fluid inclusion microthermometry and stable isotope data of the Ciurug-Cikoret veins. *Resour. Geol.*, 57, 136–148.
- Terakado, Y. and Masuda, A. (1988) The coprecipitation of rare-earth elements with calcite and aragonite. *Chem. Geol.*, 69, 103–110.
- Valley, J. (1986) Stable isotope geochemistry of metamorphic rocks. *Rev. Mineral.*, 16, 445–489.
- Warmada, I W., Lehmann, B. and Simandjuntak, M. (2003) Polymetallic sulfides and sulfosalts of the Pongkor epithermal gold-silver deposit, West Java, Indonesia. *Can. Mineral.*, 41, 185–200.
- Zheng, Y-F. (1990) Carbon-oxygen isotope covariation in hydrothermal calcite during degassing of CO₂. *Mineral. Deposita*, 25, 246–250.
- Zheng, Y.-F. (1993) Calculation of oxygen isotope fractionation in anhydrous silicate minerals. *Geochim. Cosmochim. Acta*, 57, 1079–1091.
- Zhong, S. and Mucci, A. (1995) Partitioning of rare earth elements (REEs) between calcite and seawater solutions at 25°C and 1 atm, and high dissolved REE concentrations. *Geochim. Cosmochim. Acta*, 59, 443–453.